VNU Journal of Science: Mathematics – Physics, Vol. 39, No. 2 (2023) 24-35

VNU Journal of Science: Mathematics - Physics

Journal homepage: https://js.vnu.edu.vn/MaP

Original Article

Enhancement of Methylene Blue Adsorption from ZnO/Activated Carbon Nanocompossites Prepared by Pyrolysis of Molten $ZnCl_2$ with Rice Husks

Nguyen Thi Luyen*

Thai Nguyen University of Sciences, Tan Thinh, Thai Nguyen, Vietnam

Received 11 October 2022
Revised 02 February 2023; Accepted 06 February 2023

Abstract: In this work, we synthesized a facile step pyrolysis of ZnO/activated carbon nanocomposites by using molten $ZnCl_2$ and rice husks in oxygen-limited environment. The mass ratio of molten $ZnCl_2$ and rice husks was chosen from 0 to 5 wt.%, the pyrolysis temperature range from 400 to 800 ^oC. When the mass ratio of molten $ZnCl_2$ and rice husks was equal to 1.0 and the pyrolysis temperature was at 800 ^oC, the size of ZnO nanoparticles in diameter was found to be of 10-20 nm. The ZnO/activated carbon nanocomposites exhibited a porous structure with the BET surface area, average pore diameter and pore volume of 643.9 m^2/g, 4,76 nm and 0.255 cm^3/g, respectively. To investigate the adsorption behavior of methylene blue, batch experiments were performed on all samples. The ZnO/activated carbon sample manufactured at a mass ratio of 1.0 and a pyrolysis temperature of 800 ^oC has the best methylene blue adsorption capability. The Langmuir isotherm was used to calculate the maximum adsorption capacity of methylene blue, which was 814.9 mg/g. Based on the obtained results, one can suggest that ZnO/activated carbon nanocomposites prepared by the facile pyrolysis route from molten $ZnCl_2$ and rice husks possessing eco-friendly behaviour and low productioncost can be used as a potential adsorbent for wastewater treatment.

Keywords: Rice husks, molten $ZnCl_2$, ZnO/activated carbon nanocomposites, adsorption, methylene blue, pyrolysis.

1. Introduction

Environmental pollution in the air, soil, and water are now a serious threat to life on Earth. Water pollution such as inorganic, organic, and biological pollutants, has a serious impact on human health

* Corresponding author.
E-mail address: luyennt@tnus.edu.vn

https//doi.org/10.25073/2588-1124/vnumap.4779

and the environment. So new wastewater treatment techniques and materials are being developed. The properties of activated carbon (AC) materials as adsorbents have been extensively researched in order to remove pollutants [1, 2]. AC can be produced using a variety of precursors, the most common of which are agricultural wastes such as rice husk [3-6], coconut shell [7, 8], peanut shell [9-12], crab shell [13], garlic peel [14] due to their high carbon content, abundant raw materials, low cost and friendly environment. There are two methods for preparing AC: physical activation and chemical activation [15, 16]. To avoid oxidation of carbonaceous materials, all of them were carried out in high temperature, in inert atmosphere [15]. The previous studies have shown that the chemical activation have more advantages than the physical activation due to the simpler process and high carbon content yields [15, 17, 18]. The common activating agents mixed with raw material in the chemical activation method are $ZnCl_2$ [19], $FeCl_3$ [20], KOH [21], H_3PO_4 [22] and it is usually performed in two different ways: in aqueous solution and in solid state. The mixture of activating agents with raw material in solid state using molten $ZnCl_2$ have been widely used because of its low melt point, volatility and corrosiveness at high temperatures [23], furthermore acting as a dehydrating agent which promotes the decomposition of carbonaceous material to increase the carbon content [9, 24]. Previous studies have shown that molten $ZnCl_2$ act essentially as an activating agent in the preparation of AC [9, 17, 24-27], while a few publications have detected the formation of ZnO nanoparticles on surface of activated carbon, but the reaction was performed in inert atmospheres [28, 29]. Currently, no studies have been reported on the preparation of ZnO/activated carbon nanocomposites in oxygen-limited environment using molten $ZnCl_2$ and rice husks. As a result, in this work, we show how to prepare ZnO/activated carbon nanocomposites with a high surface area and porous structure using one-step pyrolysis of molten $ZnCl_2$ and rice husks in oxygen-limited environment. We demonstrated that molten $ZnCl_2$ acts as both an activating agent and a precursor in the formation of ZnO nanoparticles on activated carbon surfaces. The ZnO/activated carbon nanocomposites are a potential adsorbent for treating polluted water. The effect of the mass ratio of molten $ZnCl_2$ and rice husks, pyrolysis temperature on the characteristics and methylene blue (MB) adsorption capacity were charaterized. The adsorption isotherm and kinetics of the organic dye MB on the prepared ZnO/activated carbon were also thoroughly investigated.

2. Materials and Methods

2.1. Materials

Zinc chloride ($ZnCl_2 \geq 98\%$), silver nitrate ($AgNO_3$, 98%), sodium hydroxide (NaOH, 97.0%), hydrochloric acid (HCl, 37%) were purchased from Sigma Aldrich Ltd, methylene blue - from China. Rice husks were collected from rice grown in Vietnam's Northern Delta, they were washed, dried, and crushed.

2.2. Synthesis of ZnO/Activated Carbon Nanocomposites

One-step pyrolysis in an oxygen-limited environment was used to prepare ZnO/activated carbon (ZnO/AC) nanocomposites. Molten $ZnCl_2$ was used as an activating agent for activated carbon as well as an initial precursor for the formation of ZnO nanoparticles. In the preparation procedure, thetemperature was fixed at 800 ^oC, the mass ratio of rice husks per molten $ZnCl_2$ was of 0, 1, 2, 3, 4 and 5 respectivelylabelled as RH0, RH1, RH2, RH3, RH4 and RH5). Set the mass ratio of molten $ZnCl_2$ to rice husks at 1, adjust the temperature between 400 and 800 ^oC (labelled RH400, RH500, RH600, RH700, RH800). The obtained product was ZnO/AC nanocomposites. To treat MB adsorption and

investigate sample characteristics, the samples were cleaned several times with distilled water and then treated with $AgNO_3$ solution until the white precipitate was gone.

2.3. Characterization Techniques

The morphology and elemental composition were characterized by a FE-SEM (Hitachi S-4800). Sample pore development was determined using N_2 adsorption/desorption isotherms at 77 K, employing a surface area analyzer (TriStar 3000 V 6.07 A). Prior to gas adsorption, the samples were degassed in a vacuum for 4 hours at 200 ^oC. The specific surface area was analyzed using the BET equation. Pore size distribution and the total pore volume of samples were estimated through the Barrett-Joyner-Halenda (BJH) method.

2.4. Batch Adsorption Experiment

The MB solution of 1000 mg/L was prepared by dissolving 1 g MB in 1,000 mL of deionized water. The working concentration was obtained by diluting it on demand, and its pH was adjusted by adding 1M NaOH or 1M HCl solution. The batch adsorption experiment was carried out in a conical flask containing 25 mg adsorbent and 25 mL MB solution in a rotary shaker under 200 rpm at 25 ^oC. The solution at defined time intervals was sampled to analyze the residual MB concentration. The filtrate was analyzed by Ultraviolet-Visible spectrophotometer (Jasco V-770, Japan) at a maximum wavelength of 664 nm. The adsorption isotherm was measured by varying the initial MB concentration in the range of 50-500 mg/L.

The removal efficiency (%) and the adsorption amount (mg/g) were calculated using the following equations, respectively:

$$H = \frac{C_0 - C_e}{C_0}.100 \quad (1)$$

$$q_e = \frac{(C_0 - C_e)V}{M} \quad (2)$$

where q_e (mg/g) is the amount of MB adsorbed on the adsorbent at equilibrium, C_0 and C_e (mg/L) are the initial concentration and the MB concentration at equilibrium, respectively, V (L) is volume of the solution, and M (g) is the mass of the adsorbent.

Adsorption kinetics

To study the adsorption process, two kinetic models were used:

Pseudo – first order equation:

$$\ln (q_e - q_t) = \ln q_e - k_1.t \quad (3)$$

Pseudo – second order equation:

$$\frac{t}{q_t} = \frac{1}{k_2.q_e^2} + \frac{1}{q_e}.t \quad (4)$$

where q_e and q_t are the adsorbent solutions at equilibrium and time t (mg g^{-1}), k_1 is the first order adsorption rate constant (min^{-1}), k_2 is the rate constant secondary adsorption (g/mg/min).

Adsorption isotherm

To study the adsorption mechanism, we used adsorption isotherm models:

$$\text{Langmuir model: } q_e = \frac{q_{max}.K_L.C_e}{1 + K_L.C_e} \quad (5)$$

$$\text{Freundlich model: } q_e = K_F.\ C_e^{1/n_F} \quad (6)$$

$$\text{Temkin model: } q_e = B_T.\ln (A_T.C_e) \quad (7)$$

where K_L, K_F are Langmuir and Freundlich adsorption constants; B_T is Temkin's constant; q_e is the adsorption capacity (mg/g); q_{max} is the maximum adsorption capacity of the adsorbent (mg/g); C_e is the concentration of the adsorbent solution; A_T is the Temkin isothermal equilibrium binding constant (L/g).

3. Results and Discussion

3.1. Structure, Morphology, Composition, Porosity of ZnO/AC Nanocomposites

Fig. 1 displayed the XRD patterns of as-prepared samples. As can be seen in Fig. 1a, XRD pattern of RH0 sample represented characteristic peaks of graphite (C) at 2Θ of 23.35°, 43.59° and 63.94° which were indexed to the (002), (100) and (110) crystaliine planes, respectively. The unsharp (002) peak reflects poor crystalities, while (100) and (110) reflections were attributed to the graphitization peaks of biochar, which was in good agreement with previous studies [30, 31]. For RH1, RH2, RH3, RH4, RH5 samples (Fig. 1a), the characteristic peaks of ZnO at 2Θ of of 31.48°, 33.93°, 35.71°, 48.88°, 57.65°, 65.53°, 68.76° and 70.25° were corresponded to the plane of (100), (002), (101), (102), (110), (103), (112) and (201) respectively, for the wurtzite structure of ZnO (JCPDS No. 36-1451). As seen in Fig. 1a, except for characteristic peaks of ZnO phase, there are observed some peaks of $Zn_5(OH)_8Cl_2.H_2O$ or simonkolleite compound (JCPDS 07-0155). This indicated that the lower or higher content of molten $ZnCl_2$ prevented the formation of ZnO nanoparticle and subsequently formed simonkolleite layered-platelet structures.

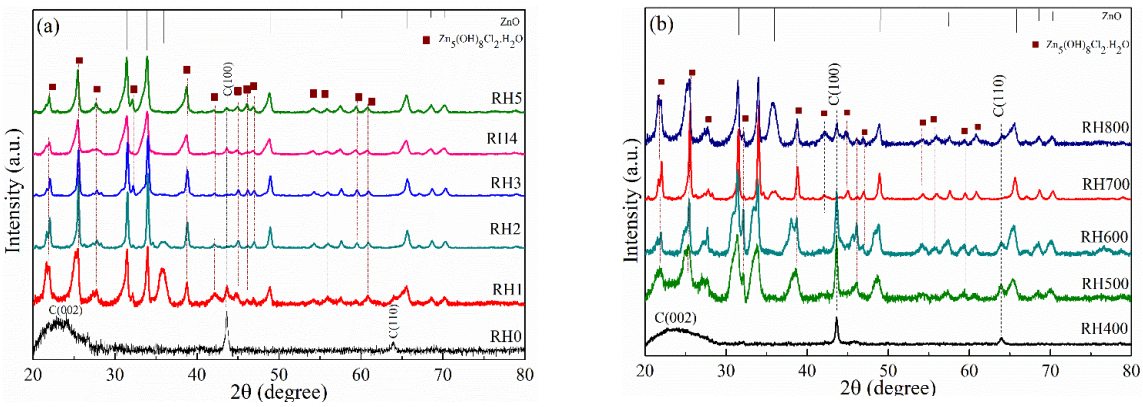

Figure 1. XRD diagram of samples synthesized at: (a) the different mass ratio of $ZnCl_2$ and rice husks, fixed of 800 °C, (b) the different pyrolysis temperature, fixed the mass ratio of $ZnCl_2$ and rice husks by 1 wt.

As displayed in Fig. 1b, activated molten $ZnCl_2$ with rice husks at 400 °C exhibited all characteristic peaks belonging to activated carbon. When pyrolysis temperature increased from 500 °C to 800 °C, there appeareds characteristic peaks of ZnO and $Zn_5(OH)_8Cl_2.H_2O$ structures on the activated carbon surface.

Fig. 2 presents FE-SEM images of RH1 sample with different image resolutions of 1 µm and 200 nm (Fig. 2a and Fig. 2b, respectively) and energy dispersive spectra (Fig. 2c).

The results showed that the ZnO nanoparticles appeared on the activated carbon surface with the particle diameters ranging from 10 to 20 nm. The ZnO nanoparticles are evenly distributed on the activated carbon surface. EDX analysis of ZnO/AC revealed that the components C, O, Zn and Ag are included with the percentage of atoms shown in Fig. 2c. The presence of Ag atom composition (0.06%) is due to the use of $AgNO_3$ solution in the cleaning process to remove excess Cl^- ions in the reaction.

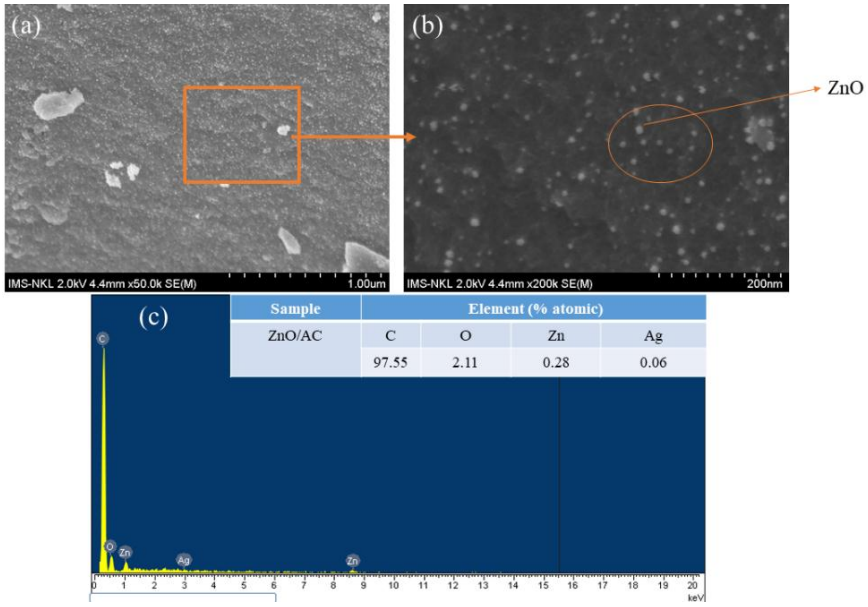

Figure 2. FE-SEM images with different image resolutions: (a) 1 µm, (b) 200 nm, and (c) EDX of RH1 sample.

Table 1. Surface area of absorbents activated by a variety of activating agents

Activating agents	The maximum surface area (m^2/g^{-1})	References
H_3PO_4	300	[32]
H_2SO_4	297	[33]
KOH	336-1824.88	[34, 35],
$ZnCl_2$	307-679	[25, 36, 37]
$FeCl_3$	505-1680	[38, 39]
$FeCl_3$ and $ZnCl_2$	1342	[39]
$ZnCl_2$	643.9	This paper

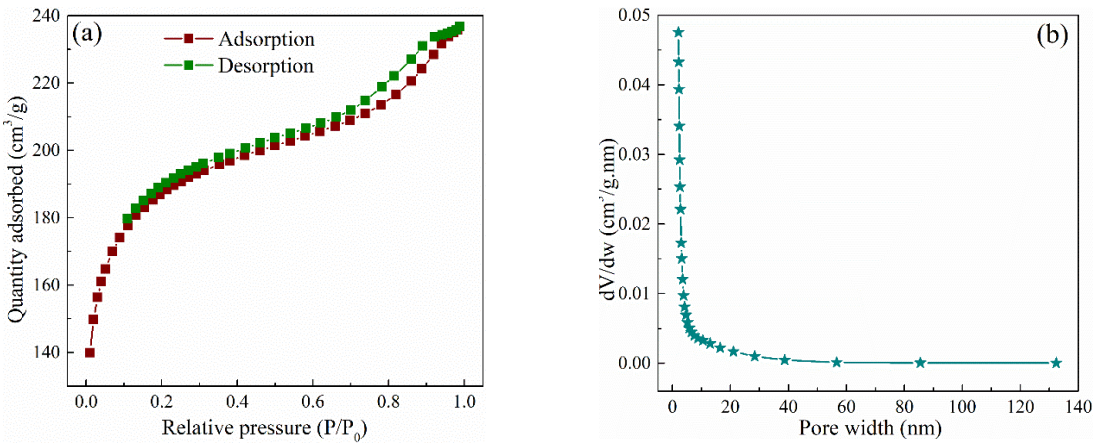

Figure 3. The N_2 adsorption-desorption isotherm at 77 K (a) and BJH pore size distribution curve of RH1 sample (b).

The porous structure of ZnO/AC was determined from the adsorption of inert gas N_2 at 77 K. Fig. 3 shows the present N_2 adsorption - desorption isotherm at 77 K (Fig. 3a) and pore size distribution according to BJH (Fig. 3b) of RH1 sample. The obtained results show that the N_2 adsorption - desorption isotherm of the ZnO/AC is IV type. The surface area, pore diameter, pore volume of ZnO/AC are 643.9 m^2/g, 4.76 nm, 0.255 cm^3/g, respectively. Table 1 compares the porosity of ZnO/AC activated by molten $ZnCl_2$ to the porosity of some other activating agents. As shown in the following section, this result also reflects the MB adsorption capacity.

3.2. Investigation of MB Adsorption Capacity

3.2.1. Effect of the Synthesis Conditions

To evaluate the MB adsorption capacity, we evaluated and compared the MB adsorption capacity of prepared ZnO/AC samples, including the influence of the mass ratio of molten $ZnCl_2$ and rice husks as well as the pyrolysis temperature. As can be seen in Fig. 4a, when inactivated with molten $ZnCl_2$ (RH0 sample), the adsorption efficiency and capacity reached values as low as 5.08% and 34.18 mg/g, respectively. Increasing the mass ratio between molten $ZnCl_2$ and rice husks from 1 to 5, the efficiency and adsorption capacity increased rapidly, reaching a maximum value of 99.35% and 693.73 mg/g when the ratio was of 1.

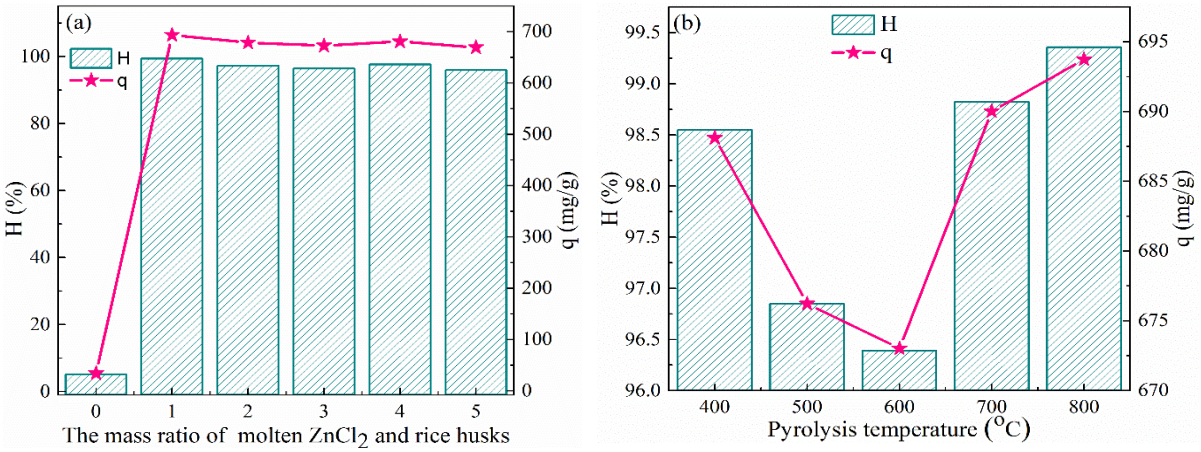

Figure 4. Effect ofthe mass ratio of molten $ZnCl_2$ and rice husks (a) andthe pyrolysis temperature on MB adsorption capacity (b).

This reflects that increasing the mass ratio of molten salt and rice husks (from 1 to 5) results in the increase of the efficiency of the molten phase and in the completion of the biomass process. This results in the increase of MB adsorption capacity. Fig. 4b depicts the effect of pyrolysis temperature ranging from 400 to 800 °C on MB adsorption capacity when the mass ratio of molten salt and rice husks is maintined at 1. The obtained results show that the adsorption capacity reaches the maximum value when the ZnO/AC is prepared at 800 °C. Previous works [40-42] have shown that the adsorption capacity of absorbents is dependent on the sample porosity, which is related to fabrication conditions such as pyrolysis temperature, pyrolysis time, carbonization source or the mass ratio of molten salt and precursor. Based on the survey results, we selected the RH1 sample for investigatigation of the influence of subsequent parameters (including pH, shaking time, initial concentration MB) on the adsorption capacity.

3.2.2. Effect of pH

Figure 5 presents the pH effect of the MB adsorption capacity. The experiments were carried out with an initial MB concentration of 200 mg/L, a shaking time of 120 minutes, a shaking speed of 200 rpm, an absorbents mass of 25 mg and a MB volume of 25 mL.

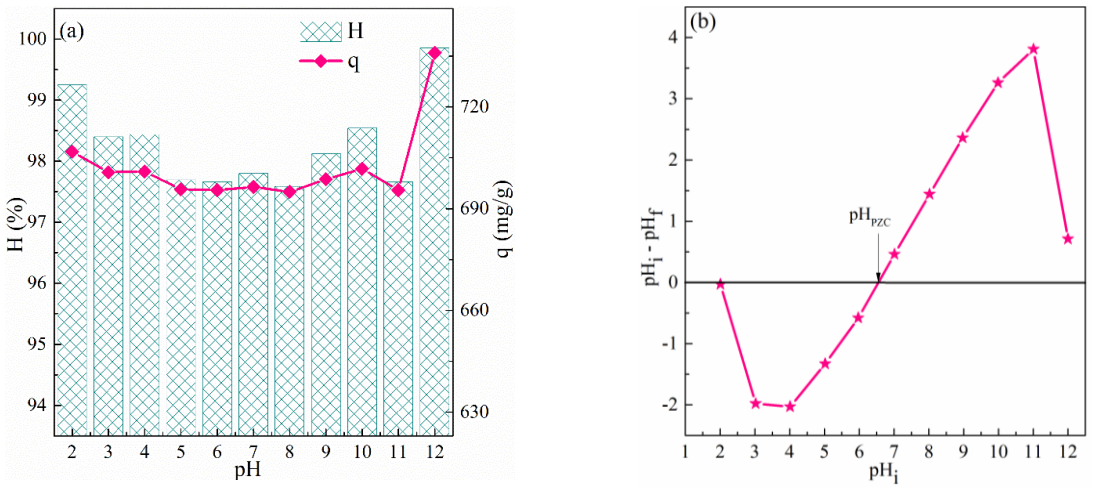

Figure 5. Effect of pH on MB adsorption capacity (a) and the point of zero charge of ZnO/AC (b).

Fig. 5a shows that the pH has no significantly affect the MB adsorption capacity, at pH 12, the MB adsorption capacity and efficiency reached maximum values of 735.94 mg/g and 99.85%, respectively. This can be explained because the solution pH is larger than pH_{PZC} (the pH_{PZC} of ZnO/AC is 6.52 in Fig. 5b), the surface of ZnO/AC is negatively charged OH^-, as a result, the electrostatic attraction between MB^+ and OH^- increased, thus the adsorption capacity increased.

3.2.3. Effect of Shaking Time

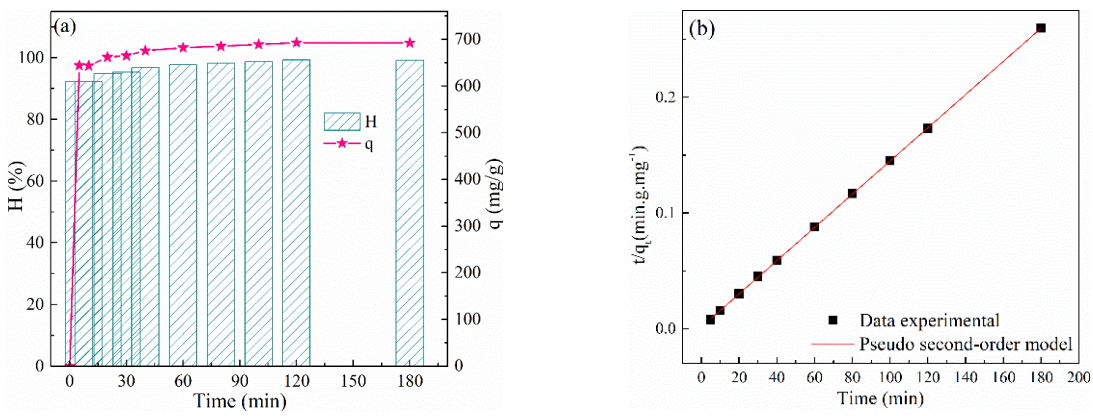

Figure 6. Effect of shaking time on MB adsorption capacity (a) andexperimental data are fitted according to the pseudo-second order model (b).

The effect of shaking time in the range from 5 to 180 minutes was also investigated in order to determine the equilibration time during the adsorption progress. The effect of the shaking time on MB

adsorption capacity is shown in Fig. 6a. The results revealed that the adsorption capacity was quickly discharged after 5 minutes, with the efficiency and MB adsorption capacity reaching 92.31% and 644.54 mg/g, respectively. From 5 to 120 minutes, the adsorption capacity increased from 644.54 mg/g to 693.11 mg/g and the efficiency increased from 92.31% to 99.27%. This can be explained by the presence of a large number of adsorption centers on the surface of the first stage absorbents. Following that, the adsorption process gradually increased until it reached equilibrium at 120 minutes. The adsorption process reached saturation between 120 and 180 minutes, possibly because the adsorption centers were gradually reduced and the resulting adsorption became stable.

To investigate the adsorption process, experimental MB adsorption of ZnO/AC was demonstrated as a function of time at an initial MB concentration of 200 mg/L and absorbents mass of 25 mg/mL. In this work, two different adsorption kinetic models were used to describe the MB adsorption process of ZnO/AC: the pseudo-first order model (Eq. 3), and the pseudo-second order model (Eq. 4). Figure 6b depicts the MB adsorption kinetics of ZnO/AC using the pseudo-second order model. The fitting results of first-order adsorption kinetics and second-order kinetics provided correlation coefficients (R^2) of 0.869 and 0.999, respectively. Among two above mentioned models, the pseudo-second order model describes the data best based on the non-linear regression coefficient (R^2). The fitting parameters are presented in Table 2.

Table 2. Fitting parameters of pseudo-second order and pseudo-first order models for the adsorption of MB onto ZnO/AC

	Pseudo second-order model			Pseudo first-order model		
$q_{e,exp}$(mg/g)	$q_{e,cal}$(mg/g)	k_2(g/mg.min)	R^2	$q_{e,cal}$(mg/g)	k_1	R^2
693.11	694.44	0.00145	0.999	100.70	0.0337	0.869

This result demonstrates that the pseudo-second order model accurately describes the MB adsorption process of ZnO/AC. This also means that the MB adsorption process is governed by chemisorption, which involves covalent bonding via electron sharing or exchange between the adsorbed and the adsorbent.

3.2.4. Effect of Initial Concentration of MB

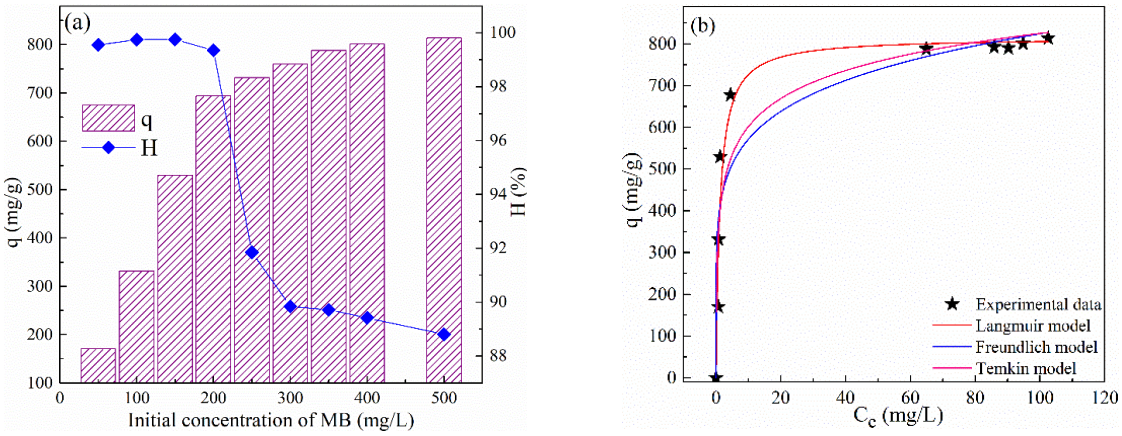

Figure 7. Effect of initial concentration MB on adsorption capacity (a) and isotherms adsorption of MB by ZnO/AC (b).

The effect of initial concentration of MB on the adsorption capacity of ZnO/AC is shown in Fig. 7a. The results showed that the adsorption capacity increased rapidly from 170.32 mg/g to 693.74 mg/g when the MB concentration increased from 50 to 200 mg/L, the large efficiency of the MB removal reached 99.76% at MB concentration of 150 mg/L. This could be because the surface adsorption sites are not occupied at the low initial MB concentration. When the initial MB concentration was increased to 500 mg/L, the MB removal efficiency decreased to 88.81%, which could be attributed to the increase in MB amount while the absorbent mass remained constant, resulting in limited adsorption sites.

To describe the MB adsorption mechanism of ZnO/AC, we use the three most general models of isotherm adsorption. These are Langmuir model (Eq. 5), Freundlich model (Eq. 6) and Temkin model (Eq. 7). Figure 7b shows the MB isotherm adsorption plot of q_e against Ce. Corresponding parameters of these models are shown in Table 3. MB adsorption data of ZnO/AC show that the correlation coefficient (R^2) when fitting according to Langmuir, Freundlich and Temkin models has the corresponding values of 0.96; 0.88; 0.9. It has been commented that the Langmuir model is the best model to describe the MB adsorption thermal equilibrium of ZnO/AC.

Table 3. Isotherm parameters of MB adsorption by ZnO/AC.

	Langmuir constants			Freundlich constants			Temkin constants		
q_{exp}(mg/g)	q_{max} (mg/g)	K_L (L/mg)	R^2	n_F	K_F (L/mg)	R^2	A_T (L/mol)	B_T (J/mol)	R^2
813.8	814.9	0.82	0.96	6.3	396.2	0.88	49.5	97	0.9

The maximum calculated adsorption capacity is 813.8 mg/g according to Langmuir model. Furthermore, the value of component 1/n is 0.159 (less than 1) according to Freundlich model. This indicates that the MB isotherm adsorption equilibrium of ZnO/AC is favorable. From these results one can suggest that the MB adsorption has occurred uniformly on the monolayer surfaces of ZnO/AC.

4. Conclusions

We synthesized ZnO/AC nanocomposites with aneffective MB adsorption capacity by a simple pyrolysis step in oxygen-limited environment, using molten $ZnCl_2$ and rice husks. ZnO/AC nanocomposites have large effective surface area, small-size pores. The effect of fabrication conditions on MB adsorption on ZnO/AC nanocomposites revealed that the optimum adsorption capacity was obtained for the samples prepared at 800 ^oC with the mass ratio of molten $ZnCl_2$ and rice husks of 1. The isotherm and kinetics of MB adsorption on ZnO/AC nanocomposites could be well fitted by the Langmuir isotherm and the pseudo-second order model, respectively. The results of this work confirmed that ZnO/AC materials have potential applications in the treatment of pollutants in environment.

Acknowledgment

This work was financially supported by the Ministry of Education and Training of Vietnam (Code B2021-TNA-16).

References

[1] S. R. Sánchez, B. Ruiz, D. M. Blanco, M. S. Arenillas, M. A. Diez, I. S. Ruiz, J. F. Marco, J. Blanco, E. Fuente, Sustainable Thermochemical Single-Step Process to Obtain Magnetic Activated Carbons from Chestnut Industrial

Wastes, ACS Sustain. Chem. Eng, Vol. 7, 2019, pp. 17293-17305, https://doi.org/10.1021/acssuschemeng.9b04141.

[2] S. Guo, J. Peng, W. Li, K. Yang, L. Zhang, S. Zhang, H. Xia, Effects of CO_2 Activation on Porous Structures of Coconut Shell-based Activated Carbons, Appl. Surf. Sci, Vol. 255, 2009, pp. 8443-8449, https://doi.org/10.1016/j.apsusc.2009.05.150.

[3] J. Lou, X. Xu, Y. Gao, D. Zheng, J. Wang, Z. Li, Preparation of Magnetic Activated Carbon from Waste Rice Husk for the Determination of Tetracycline Antibiotics in Water Samples, RSC Adv, Vol. 6, 2016, pp. 112166-112174, https://doi.org/10.1039/c6ra24397e.

[4] Riyanto, R. Astuti, B. I. Mukti, Simple Preparation of Rice Husk Activated Carbon (RHAC) and Applications for Laundry and Methylene Blue Wastewater Treatment, AIP Conf. Proc, 2017, pp. 1911, https://doi.org/10.1063/1.5016027.

[5] K. L. Van, T. T. L. Thi, Activated Carbon Derived from Rice Husk by Naoh Activation and Its Application in Supercapacitor, Prog. Nat. Sci. Mater. Int, Vol. 24, 2014, pp. 191-198, https://doi.org/10.1016/j.pnsc.2014.05.012.

[6] M. Ahiduzzaman, A. K. M. S. Islam, Preparation of Porous Biochar and Activated Carbon from Rice Husk by Leaching Ash and Chemical Activation, Springerplus, Vol. 5, 2016, https://doi.org/10.1186/s40064-016-2932-8.

[7] M. K. B. Gratuito, T. Panyathanmaporn, R. A. Chumnanklang, N. Sirinuntawittaya, A. Dutta, Production of Activated Carbon from Coconut Shell: Optimization Using Response Surface Methodology, Bioresour, Technol, Vol. 99, 2008, pp. 4887-4895, https://doi.org/10.1016/j.biortech.2007.09.042.

[8] W. M. A. W. Daud, W. S. W. Ali, Comparison on Pore Development of Activated Carbon Produced from Palm Shell and Coconut Shell, Bioresour, Technol, Vol. 93, 2004, pp. 63-69, https://doi.org/10.1016/j.biortech.2003.09.015.

[9] H. Shang, Y. Lu, F. Zhao, C. Chao, B. Zhang, H. Zhang, Preparing High Surface Area Porous Carbon from Biomass by Carbonization in A Molten Salt Medium, RSC Adv, Vol. 5, 2015, pp. 75728-75734, https://doi.org/10.1039/c5ra12406a.

[10] J. Gülen, F. Zorbay, Methylene Blue Adsorption on a Low Cost Adsorbent-Carbonized Peanut Shell, Water Environ. Res, Vol. 89, 2017, pp. 805-816, https://doi.org/10.2175/106143017x14902968254836.

[11] R. Li, Y. Zhang, W. Chu, Z. Chen, J. Wang, Adsorptive Removal of Antibiotics from Water using Peanut Shells from Agricultural Waste, RSC Adv, Vol. 8, 2018, pp. 13546-13555, https://doi.org/10.1039/c7ra11796e.

[12] W. Cai, Z. Li, J. Wei, Y. Liu, Synthesis of Peanut Shell Based Magnetic Activated Carbon with Excellent Adsorption Performance Towards Electroplating Wastewater, Chem. Eng. Res. Des, Vol. 140, 2018, pp. 23-32, https://doi.org/10.1016/j.cherd.2018.10.008.

[13] Y. Gao, Q. Yue, B. Gao, High Surface Area and Oxygen-enriched Activated Carbon Synthesized from Animal Cellulose and Evaluated in Electric Double-layer Capacitors, RSC Adv, Vol. 5, 2015, pp. 31375-31383, https://doi.org/10.1039/c4ra16965d.

[14] G. G. Huang, Y. F. Liu, X. X. Wu, J. J. Cai, Activated Carbons Prepared by the KOH Activation of A Hydrochar from Garlic Peel and Their CO_2 Adsorption Performance, Xinxing Tan Cailiao/New Carbon Mater, Vol. 34, 2019, pp. 247-257, https://doi.org/10.1016/S1872-5805(19)60014-4.

[15] J. Bedia, M. P. Garzón, A. G. Avilés, J. J. Rodriguez, C. Belver, Review on Activated Carbons by Chemical Activation with $FeCl_3$, CJ. Carbon Res, Vol. 6, 2020, pp. 21, https://doi.org/10.3390/c6020021.

[16] J. Bedia, C. Belver, S. Ponce, J. Rodriguez, J. J. Rodriguez, Adsorption of Antipyrine by Activated Carbons from $FeCl_3$-activation of Tara Gum, Chem. Eng. J, Vol. 333, 2018, pp. 58-65, https://doi.org/10.1016/j.cej.2017.09.161.

[17] X. Wang, J. S. Lee, C. Tsouris, D. W. DePaoli, S. Dai, Preparation of activated Mesoporous Carbons for Electrosorption of Ions From Aqueous Solutions, J. Mater. Chem, Vol. 20, 2010, pp. 4602-4608, https://doi.org/10.1039/b925957k.

[18] A. Lazzarini, A. Piovano, R. Pellegrini, G. Leofanti, G. Agostini, S. Rudić, M. R. Chierotti, R. Gobetto, A. Battiato, G. Spoto, A. Zecchina, C. Lamberti, E. Groppo, A Comprehensive Approach to Investigate the Structural and Surface Properties of Activated Carbons and Related Pd-based Catalysts, Catal. Sci. Technol, Vol. 6, 2016, pp. 4910-4922, https://doi.org/10.1039/c6cy00159a.

[19] B. Li, J. Hu, H. Xiong, Y. Xiao, Application and Properties of Microporous Carbons Activated by $ZnCl_2$: Adsorption Behavior and Activation Mechanism, ACS Omega, Vol. 5, 2020, pp. 9398-9407, https://doi.org/10.1021/acsomega.0c00461.

[20] K. M. Watts, E. Adewakun, O. Norouzi, T. D. Abhi, R. Pradhan, A. Dutta, Effects of $FeCl_3$ Catalytic Hydrothermal Carbonization on Chemical Activation of Corn Wet Distillers' Fiber, ACS Omega, Vol. 6, 2021, pp. 14875-14886, https://doi.org/10.1021/acsomega.1c00557.

[21] J. Hou, J. Hou, Y. Liu, S. Wen, W. Li, R. Liao, L. Wang, Sorghum-waste-derived High-surface Area KOH-Activated Porous Carbon for Highly Efficient Methylene Blue and Pb(II) Removal, ACS Omega, Vol. 5, 2020, pp. 13548-13556, https://doi.org/10.1021/acsomega.9b04452.

[22] O. Oginni, K. Singh, G. Oporto, B. D. Andoh, L. McDonald, E. Sabolsky, Effect of One-step and Two-step H_3PO_4 Activation on Activated Carbon Characteristics, Bioresour. Technol. Reports, Vol. 8, 2019, pp. 100307, https://doi.org/10.1016/j.biteb.2019.100307.

[23] F. Zhang, L. Liu, L. Chen, Y. Shi, A Cellulose Dissolution and Encapsulation Strategy to Prepare Carbon Nanospheres with Ultra-small Size and High Nitrogen Content for the Oxygen Reduction Reaction, New J. Chem, Vol. 44, 2020, pp. 10613-10620, https://doi.org/10.1039/d0nj01659d.

[24] A. Özhan, Ö. Şahin, M. M. Kuşuk, C Saka, Preparation and Characterization of Activated Carbon from Pine Cone by Microwave-induced $ZnCl_2$ Activation and its Effects on the Adsorption of Methylene Blue, Cellulose, Vol. 21, 2014, pp. 2457-2467, https://doi.org/10.1007/s10570-014-0299-y.

[25] G. S. D. Reis, M. Wilhelm, T. C. D. A. Silva, K. Rezwan, C. H. Sampaio, E. C. Lima, S. M. A. G. U. D. Souza, The use of Design of Experiments for the Evaluation of the Production of Surface Rich Activated Carbon from Sewage Sludge Via Microwave and Conventional Pyrolysis, Appl. Therm. Eng, Vol. 93, 2016, pp. 590-597, https://doi.org/10.1016/j.applthermaleng.2015.09.035.

[26] G. Duman, Y. Onal, C. Okutucu, S. Onenc, J. Yanik, Production of Activated Carbon from Pine Cone and Evaluation of Its Physical, Chemical, and Adsorption Properties, Energy and Fuels, Vol. 23, 2009, pp. 2197-2204, https://doi.org/10.1021/ef800510m.

[27] M. O. Marín, C. F. González, A. M. García, V. G. Serrano, Preparation of Activated Carbon from Cherry Stones by Chemical Activation with $ZnCl_2$, Appl. Surf. Sci, Vol. 252, 2006, pp. 5967-5971, https://doi.org/10.1016/j.apsusc.2005.11.008.

[28] L. Wang, P. Zhou, Y. Guo, J. Zhang, X. Qiu, Y. Guan, M. Yu, H. Zhu, Q. Zhang, The Effect of $ZnCl_2$ Activation on Microwave Absorbing Performance in Walnut Shell-derived Nano-porous Carbon, RSC Adv, Vol. 9, 2019, pp. 9718-9728, https://doi.org/10.1039/c8ra09932d.

[29] R. Madhu, V. Veeramani, S. M. Chen, P. Veerakumar, S. B. Liu, N. Miyamoto, Functional Porous Carbon-ZnO Nanocomposites for High-performance Biosensors and Energy Storage Applications, Phys. Chem. Chem. Phys, Vol. 18, 2016, pp. 16466-16475, https://doi.org/10.1039/c6cp01285j.

[30] A. P. S. Chauhan, K. Chawla, Comparative Studies on Graphite and Carbon Black Powders, and Their Dispersions, J. Mol. Liq, Vol. 221, 2016, pp. 292-297, https://doi.org/10.1016/j.molliq.2016.05.043.

[31] M. Pawlyta, J. N. Rouzaud, S. Duber, Raman Microspectroscopy Characterization of Carbon Blacks: Spectral Analysis and Structural Information, Carbon N. Y, Vol. 84, 2015, pp. 479-490, https://doi.org/10.1016/j.carbon.2014.12.030.

[32] T. Boualem, A. Debab, A. M. D. Yuso, M. T. Izquierdo, Activated Carbons Obtained from Sewage Sludge by Chemical Activation: Gas-Phase Environmental Applications, J. Environ. Manage, Vol. 140, pp. 145-151, https://doi.org/10.1016/j.jenvman.2014.03.016.

[33] Z. Tang, C. Cen, P. Fang, Y. Liang, Preparation and Characterization of Sewage Sludge-based Activated Carbon, Adv. Mater. Res, Vol. 599, 2012, pp. 614-617, https://doi.org/10.4028/www.scientific.net/AMR.599.614.

[34] E. Kacan, Optimum BET Surface Areas for Activated Carbon Produced from Textile Sewage Sludges and Its Application as Dye Removal, J. Environ. Manage, Vol. 166, 2016, pp. 116-123, https://doi.org/10.1016/j.jenvman.2015.09.044.

[35] M. J. Ahmed, S. K. Theydan, Microporous Activated Carbon from Siris Seed Pods by Microwave-induced KOH Activation for Metronidazole Adsorption, J. Anal. Appl. Pyrolysis, Vol. 99, 2013, pp. 101-109, https://doi.org/10.1016/j.jaap.2012.10.019.

[36] D. Sheha, H. Khalaf, N. Daghestani, Experimental Design Methodology for the Preparation of Activated Carbon from Sewage Sludge by Chemical Activation Process, Arab. J. Sci. Eng. Vol. 38, 2013, pp. 2941-2951, https://doi.org/10.1007/s13369-012-0470-4.

[37] X. Wang, X. Liang, Y. Wang, X. Wang, M. Liu, D. Yin, S. Xia, J. Zhao, Y. Zhang, Adsorption of Copper (II) Onto Activated Carbons from Sewage Sludge by Microwave-induced Phosphoric Acid and Zinc Chloride Activation, Desalination. Vol. 278, 2011, pp. 231-237, https://doi.org/10.1016/j.desal.2011.05.033.

[38] J. Bedia, C. Belver, S. Ponce, J. Rodriguez, J. J. Rodriguez, Adsorption of Antipyrine by Activated Carbons from $FeCl_3$-Activation of Tara Gum, Chem. Eng. J, Vol. 333, 2018, pp. 58-65, https://doi.org/10.1016/j.cej.2017.09.161.

[39] D. Tian, Z. Xu, D. Zhang, W. Chen, J. Cai, H. Deng, Z. Sun, Y. Zhou, Micro-mesoporous Carbon from Cotton Waste Activated by $Fecl_3/Zncl_2$: Preparation, Optimization, Characterization and Adsorption of Methylene Blue and Eriochrome Black T, J. Solid State Chem, Vol. 269, 2019, pp. 580-587, https://doi.org/10.1016/j.jssc.2018.10.035.

[40] C. Zhao, B. Wang, B. K. G. Theng, P. Wu, F. Liu, S. Wang, X. Lee, M. Chen, L. Li, X. Zhang, Formation and mechanisms of Nano-metal Oxide-biochar Composites For Pollutants Removal: A Review, Sci. Total Environ, Vol. 767, 2021, pp. 145305, https://doi.org/10.1016/j.scitotenv.2021.145305.

[41] Y. Xiang, X. Yang, Z. Xu, W. Hu, Y. Zhou, Z. Wan, Y. Yang, Y. Wei, J. Yang, D. C. W. Tsang, Fabrication of Sustainable Manganese Ferrite Modified Biochar from Vinasse for Enhanced Adsorption of Fluoroquinolone Antibiotics: Effects and mechanisms, Sci. Total Environ, Vol. 709, 2020, pp. 136079, https://doi.org/10.1016/j.scitotenv.2019.136079.

[42] Y. Wang, L. Wang, X. Deng, H. Gao, A Facile Pyrolysis Synthesis of Biochar/Zno Passivator: Immobilization Behavior and Mechanisms for Cu (II) in Soil, Environ. Sci. Pollut. Res, Vol. 27, 2020, pp. 1888-1897, https://doi.org/10.1007/s11356-019-06888-z.